with single-crystal silicon (~$0.05/cm³ compared with ~$2.5/cm³). Most important, it has a low Young's modulus, which allows actuation even of small area devices. Pneumatically actuated valves and pumps will be useful for a wide variety of fluidic manipulation for lab-on-a-chip applications. In the future, it should be possible to design electrically or magnetically actuated valves and pumps that can be used as implantable devices for clinical applications.

Note added in proof: After submission of this manuscript, we learned of related work by J. Anderson *et al.* in the Whitesides group at Harvard University.

References and Notes

1. L. M. Roylance and J. B. Angell, *IEEE Trans. Electron Devices* **ED-26**, 1911 (1979).
2. N. Yazdi, F. Ayazi, K. Najafi, *Proc. IEEE* **86**, 1640 (1998).
3. O. N. Tufte, P. W. Chapman, D. Long, *J. Appl. Phys.* **33**, 3322 (1962).
4. L. Kuhn, E. Bassous, R. Lane, *IEEE Trans. Electron Devices* **ED-25**, 1257 (1978).
5. L. Y. Lin, E. L. Goldstein, R. W. Tkach, *IEEE J. Selected Top. Quantum Electron.* **5**, 4 (1999).
6. R. S. Muller and K. Y. Lau, *Proc. IEEE* **86**, 1705 (1998).
7. L. J. Hornbeck and W. E. Nelson, *OSA Tech. Dig. Ser.* **8**, 107 (1988).
8. D. J. Harrison *et al.*, *Science* **261**, 895 (1993).
9. S. C. Jacobson, R. Hergenroder, L. B. Koutny, J. M. Ramsey, *Anal. Chem.* **66**, 1114 (1994).
10. M. U. Kopp, A. J. de Mello, A. Manz, *Science* **280**, 1046 (1998).
11. S. Shoji, *Top. Curr. Chem.* **194**, 163 (1998).
12. P. Gravesen, J. Branebjerg, O. S. Jensen, *J. Micromech. Microeng.* **3**, 168 (1993).
13. L. Buchaillot, E. Farnault, M. Hoummady, H. Fujita, *Jpn. J. Appl. Phys. 2* **36**, L794 (1997).
14. Y. N. Xia *et al.*, *Science* **273**, 347 (1996).
15. Y. N. Xia and G. M. Whitesides, *Angew. Chem. Int. Ed. Engl.* **37**, 550 (1998).
16. C. S. Effenhauser, G. J. M. Bruin, A. Paulus, M. Ehrat, *Anal. Chem.* **69**, 3451 (1997).
17. E. Delamarche, A. Bernard, H. Schmid, B. Michel, H. Biebuyck, *Science* **276**, 779 (1997).
18. A. Y. Fu, C. Spence, A. Scherer, F. H. Arnold, S. R. Quake, *Nature Biotechnol.* **17**, 1109 (1999).
19. K. Hosokawa, T. Fujii, I. Endo, *Anal. Chem.* **71**, 4781 (1999).
20. D. C. Duffy, O. J. A. Schueller, S. T. Brittain, G. M. Whitesides, *J. Micromech. Microeng.* **9**, 211 (1999).
21. D. C. Duffy, J. C. McDonald, O. J. A. Schueller, G. M. Whitesides, *Anal. Chem.* **70**, 4974 (1998).
22. P. J. A. Kenis, R. F. Ismagilov, G. M. Whitesides, *Science* **285**, 83 (1999).
23. For multilayers, a thick layer was prepared as previously described; each thin layer was baked at 80°C for 20 min. The growing thick layer was assembled on each new thin layer and bonded by baking at 80°C for 20 min. Seven-layer devices have been produced by this method; no obvious limitations exist to limit the number of layers.
24. J. C. Lötters, W. Olthuis, P. H. Veltink, P. Bergveld, *J. Micromech. Microeng.* **7**, 145 (1997).
25. Conductive silicone was created by the addition of a fine carbon black (Vulcan XC72; Cabot, Billerica, MA) at 10% or higher concentration by weight. Conductivity increased with carbon black concentration from 5.6×10^{-16} to ~5×10^{-3} (ohm·cm)$^{-1}$. Magnetic silicone was created by the addition of iron powder (~1 μm particle size); up to 20% Fe by weight was added. For both conductive and magnetic silicones, multilayer bonding functioned normally.
26. K. Ikuta, K. Hirowatari, T. Ogata, in *Proceedings IEEE International MEMS 94 Conference* (IEEE, Piscataway, NJ, 1994), pp. 1–6.
27. R. B. M. Schasfoort, S. Schlautmann, J. Hendrikse, A. van den Berg, *Science* **286**, 942 (1999).
28. S. C. Jacobson, T. E. McKnight, J. M. Ramsey, *Anal. Chem.* **71**, 4455 (1999).
29. C. S. Effenhauser, G. J. M. Bruin, A. Paulus, *Electrophoresis* **18**, 2203 (1997).
30. M. Washizu, S. Suzuki, O. Kurosawa, T. Nishizaka, T. Shinohara, *IEEE Trans. Ind. Appl.* **30**, 835 (1994).
31. R. Pethig and G. H. Markx, *Trends Biotechnol.* **15**, 426 (1997).
32. R. Brechtel, W. Hoffmann, H. Rudiger, H. Watzig, *J. Chromatogr. A* **716**, 97 (1995).
33. C. A. Lucy and R. S. Underhill, *Anal. Chem.* **68**, 300 (1996).
34. The magnitude of flow (and even its direction) depends in a complicated fashion on ionic strength and type, the presence of surfactants, and the charge on the walls of the flow channel; furthermore, because electrolysis is taking place continuously, the capacity of buffer to resist pH changes is finite. Precise control of flow thus requires calibration for each new buffer or solute and can be difficult when the exact composition of a sample is not known in advance. Electroosmotic flow can also induce unwanted electrophoretic separation of molecules, creating demixing problems. Dielectrophoresis does not require electrolysis and therefore does not cause bubble formation but still suffers from sample and solvent sensitivity.
35. Each control channel was connected to the common port of a miniature three-way switch valve (LHDA1211111H; Lee Valve, Westbrook, CT), powered by a fast Zener-diode circuit and controlled by a digital data acquisition card (AT-DIO-32HS; National Instruments, Austin, TX). Regulated external pressure was provided to the normally closed port, allowing the control channel to be pressurized or vented to atmosphere by switching the miniature valve.
36. If one used another actuation method that did not suffer from opening and closing lag, this valve would run at ~375 Hz. The spring constant can be adjusted by changing the membrane thickness; this allows optimization for either fast opening or fast closing.
37. *E. coli* were pumped at 10 Hz through the channel. Samples of known volume were taken from the output well (pumped) and the input well (control), and serial dilutions of each were plated on Luria-Bertani agar plates and grown overnight at 37°C. Viability was assessed by counting colonies in the control and pumped samples and correcting for sample volumes and dilution.
38. J. Fahrenberg *et al.*, *J. Micromech. Microeng.* **5**, 77 (1995).
39. C. Goll *et al.*, *J. Micromech. Microeng.* **6**, 77 (1996).
40. X. Yang, C. Grosjean, Y. C. Tai, C. M. Ho, *Sensors Actuators A* **64**, 101 (1998).
41. A. M. Young, T. M. Bloomstein, S. T. Palmacci, *J. Biomech. Eng. Trans. ASME* **121**, 2 (1999).
42. This work was partially supported by NIH (NS-11756, DA-9121).

Chain Mobility in the Amorphous Region of Nylon 6 Observed under Active Uniaxial Deformation

Leslie S. Loo, Robert E. Cohen, Karen K. Gleason*

A specially designed solid-state deuterium nuclear magnetic resonance probe was used to examine the effect of uniaxial elongation on the chain mobility in the amorphous region of semicrystalline nylon 6. In measurements conducted near the glass transition temperature, there was measurable deformation-induced enhancement of the mobility of the amorphous chains up to the yield point. This enhanced mobility decayed once deformation was stopped. Enhanced mobility was not observed in deformation at room temperature. The mechanics of deformation can be explained by the Robertson model for glassy polymers near the glass transition temperature, which states that applied stress induces liquid-like behavior in the polymer chains.

Polymers are gradually replacing metals in many important engineering applications. Ongoing research seeks methodologies to design polymers with improved mechanical properties without sacrificing the advantages of low density and ease of processing. This task requires knowledge of deformation mechanisms, which are well understood in metals but less so in thermoplastic polymers. Various models have been proposed to account for plastic deformation in amorphous glassy polymers (*1, 2*). It is unclear whether such models can be used to characterize the behavior in the amorphous region of semicrystalline polymers, such as nylon, because the presence of crystallites imposes topological constraints on the chains in the amorphous zones (*3, 4*).

Experimental elucidation of the deformation mechanism in polymers has focused on reconstructing the phenomenon on the basis of x-ray or nuclear magnetic resonance (NMR) measurements of the orientation or dynamics of the polymer after deformation has ceased, that is, in a "dead" polymer specimen (*5, 6*). Thus, any motions that may be activated by steady deformation or during yield would not be observed. Furthermore, the lack of long-range order in the amorphous regions of semicrystalline polymers precludes in-depth investigation by x-ray tech-

Department of Chemical Engineering and Center for Materials Science and Engineering, Massachusetts Institute of Technology, Cambridge, MA 02139, USA.

*To whom correspondence should be addressed. E-mail: kkgleasn@mit.edu

niques. Hence, a method to probe the detailed chain dynamics associated with active macroscopic deformation is desirable.

Deuterium NMR is a powerful technique for probing molecular motions in polymers (7). It has been used to analyze the effect of static loads on chain mobility for highly crystalline poly(p-phenyleneterephthalamide) (8). The only simultaneous deuterium NMR and active deformation experiment performed thus far is by Hansen et al. (9), who examined the mobility of phenyl groups in amorphous polycarbonate during small strain (a few percent) deformation. In order to observe the dynamical processes activated during polymer deformation in the moderate to large strain (up to 100%) regimes, we constructed a deuterium NMR probe (10) to detect the molecular-scale processes that occurr in polymer rods undergoing uniaxial tensile deformation.

Nylon 6 cylindrical rods (3-mm diameter, 30% crystallinity) were immersed in D_2O at $21° \pm 1°C$ for several weeks. This process leads to exchange of D for H only in the NH bonds (11–13) of the amorphous regions (Fig. 1). The deuterated rods were held in vacuum at 80°C for 2 days and were subsequently stored in a dessicator at $21° \pm 1°C$ before their use in strain and NMR experiments. The glass transition temperature (T_g) of the rods conditioned in this way is 69°C, as determined by differential scanning calorimetry measurements at 5°C/min.

The uniaxial tensile experiment was performed in an environmental chamber with a N_2 purge on an Instron 4201 machine to obtain the stress-strain curve. The gauge length of each sample was 12 mm. Tests were performed at an elongation rate of 0.06 mm/min, at both room temperature and $70° \pm 1°C$. The NMR analysis was done at 45.8 MHz for deuterium. A quadrupolar pulse sequence [$90°x - \tau_1 - 90°y - \tau_2 - Acq$] with CYCLOPS (14, 15) phase cycling was used with a 90° pulse width of 2.5 to 2.6 μs. The digitization rate used was 0.5 μs with a total acquisition time of 512 μs. The recycle delay was 0.1 s, and 9600 scans were needed for each spectrum. The nylon 6 rod axis coincides with the stretching axis, and they are both perpendicular to the static magnetic field. The experiments were also done with a N_2 purge.

A plot of engineering stress (left axis) and engineering strain (right axis) versus time of deuterated nylon 6, obtained from a typical Instron experiment at $T = 70°C$, is shown in Fig. 2A. (Engineering strain, ε, is defined as $\varepsilon = \Delta L/L_0$, where ΔL is the increase in length and L_0 is the initial length of the sample; engineering stress is the observed force divided by the original undeformed cross-sectional area.) The stress-time curve shows a yield point, yield drop, and strain hardening. A similar curve is also obtained for a specimen deformed at room

temperature with a yield stress of 75 MPa at a strain of 0.17 and yield drop to 61 MPa at a strain of 0.42. The sample that deformed at 70°C has a lower modulus and yield point, which is expected because of the softening of the amorphous regions at the higher temperature. Homogeneous deformation was observed in all of the samples up to the yield point, after which necking (a narrowing of the sample width) occurred. Initial and final specimen shapes are shown in Fig. 2.

A series of room-temperature deuterium NMR spectra of the amorphous region of nylon 6 as a function of strain is shown in Fig. 3A. Each spectrum was accumulated during a period of ~18 min while the sample was deforming continuously from $\varepsilon = 0$ to 0.83. Changes in the spectra reflect those undergone by the deuterated chains in the amorphous region; if chains from the crystalline regions are drawn into the noncrystalline region by the deformation, they will not be observed by NMR because they are not deuterated. The undeformed material has a characteristic Pake pattern with quadrupolar coupling constant of 191 kHz and asymmetry parameter of 0.17 (12) with very little motional averaging of the ND bonds in the amorphous region. The horns and feet (see Fig. 3A) of the spectra are signals arising from ND bond vectors that are nearly perpendicular and parallel to the static magnetic field, respectively. The areas of the spectra decrease with increasing strain as the specimen deformed and was drawn out of the coil volume. The intensity of the height of the horn relative to the center also decreases with strain. The spectra of the sample at selected strains normalized by area are shown in Fig. 3B. At small strains (<0.3), where necking has not yet occurred, the line shapes are similar to that of the undeformed sample, implying little, if any, change in mobility and orientation of the deuterium atoms in the amorphous regions during deformation. At high strains (>0.5), the line shapes are a complex combination of components from the neck and its shoulders (unnecked regions adjacent to the neck), as well as the unnecked regions near the grips. Broader horns and
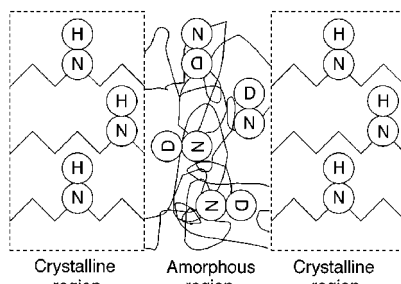
higher relative heights of the feet and center are observed compared to the undeformed sample. These changes are attributed to the orientation of the ND bonds aligning perpendicular to the rod axis as the chains in the amorphous regions align parallel to the draw direction in the neck and shoulder regions.

Spectra of deuterated nylon 6 undergoing deformation at the same elongation rate (0.06 mm/min), but at 70°C, are shown in Fig. 3C. The line shape of the undeformed sample is similar to that at room temperature, except for the very pronounced center peak, which indicates the presence of a population of highly mobile deuterons at the higher temperature. The narrow ^2H NMR line shape corresponds to motional averaging at a frequency >200 kHz. The intensity of the central narrow peak increases at small strains, indicating an increase of mobility in the amorphous regions. The variation of the ratio of the height of the center peak to the height of the horns with strain for two series of spectra performed under nominally identical conditions is shown in Fig. 2B. (The center peak height is a measure of the number of ND groups with
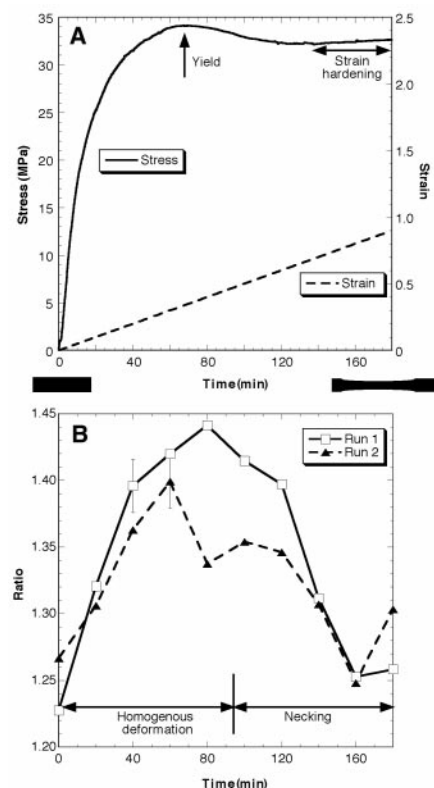

Fig. 2. (**A**) Plot of engineering stress (left axis) and engineering strain (right axis) versus time of deuterated nylon 6 elongated at 0.06 mm/ min at 70°C. (**B**) Plot of the ratio of the height of the center peak to the height of the horns versus strain for two series of deuterium NMR spectra at 70°C. A representative error bar for each run is shown. The initial (left) and final (right) shapes of the nylon 6 specimen are shown (black bars between the panels).

Fig. 1. Simplified picture of crystalline and amorphous regions in nylon 6 indicating the locations of the ND bonds.

Fig. 3. (**A**) Deuterium NMR spectra of deuterated nylon 6 rod undergoing active tensile deformation at room temperature and (**B**) normalized by area. The corresponding strains are shown to the left of each spectrum. The elongation rate is 0.06 mm/min. Each spectrum is the accumulation of 9600 scans with a digitization rate of 0.5 μs. (**C**) As in (A) but at 70°C.

Fig. 4. Plot of (**A**) engineering stress (left axis) and engineering strain (right axis) versus time of deuterated nylon 6 elongated at 0.06 mm/min at 70°C with 1 hour of relaxation at a strain of 0.36 and (**B**) ratio of the height of the center peak to the height of the horns versus strain. Duplicate runs are shown. A representative error bar for each run is shown.
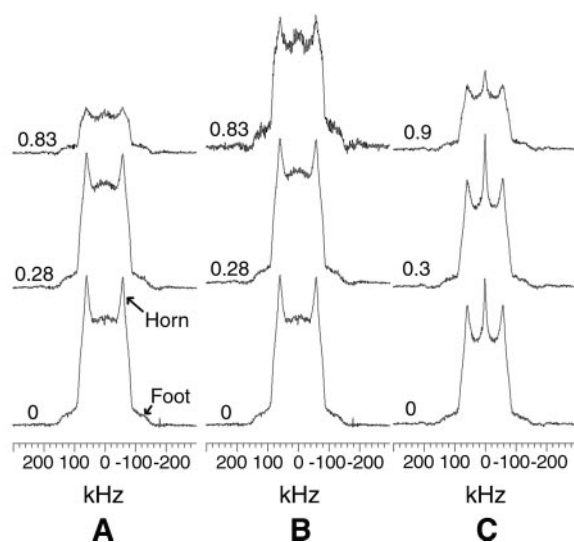
high mobility, whereas the horn height is a measure of the number of "static" ND groups. We chose to use this ratio because of the different line widths of the central peak and horns and because of the difficulty in simulating the deuterium spectra when both partial motional averaging and anisotropy are present.) Up to the yield point (strain ~ 0.4), the ratio of center peak height to horn height increases monotonically, whereas little change in the broad component of the deuterium line shape is observed. This analysis reveals that the active deformation enhances the mobility of the deuterons in the amorphous regions in the small to moderate strain regime. The maximum fractional increase of the center peak area (relative to the entire deuterium NMR signal) is 1%, thereby showing NMR to be a superior technique in detecting such small changes in mobility. Beyond the yield point, the specimen becomes necked and is no longer spatially uniform. Most of the deformation in the necked specimen becomes localized in small regions in the shoulders, while the central shaft of the entire specimen deforms no further. Thus, the amount of material in the specimen which experiences mobility enhancement drops and the static fraction increases. As in the room temperature experiment, the static component of the line shape at high strain displays higher relative heights of the feet compared to the undeformed rod, because of the alignment of the nylon chains along the draw axis in the neck and shoulders. At strains beyond the onset of necking, the complexity of the line shapes, which are a superposition of several components, precludes a simple analysis of the results.

In order to ascertain the nature of the mobility enhancement at 70°C, another experiment was performed whereby the deformation was stopped at a (preneck) strain of 0.36; the specimen was then held at constant length for 1 hour, and deformation was then resumed. Tensile experiments were carried out on both the Instron and the NMR probe. The variation of the engineering stress and engineering strain with time for two repetitions of the interrupted deformation experiment is shown in Fig. 4A. The ^{2}H NMR spectra were similar to those of Fig. 3C, and the ratio of the height of the center peak to that of the horns of two separate runs were plotted in Fig. 4B. Again, up to the yield point, this ratio increases with time (or strain). However, when deformation ceased and the specimen was held at a fixed strain, this ratio decreased with time as the stress relaxed. When deformation recommenced, the stress rose and the ratio of the center peak height to the horn height immediately increased. This result shows that the enhancement in mobility of the deuterons is due to the process of active deformation in the material.

This behavior is consistent with the Robertson model (*16*), which was proposed to account for yielding in glassy polymers. This model states that the applied stress increases mobility to liquid-like values associated with a fictive temperature that is above the glass transition temperature. The model accounts for the increase in intensity of the mobile peak at low strains in the 70°C experiment when the sample deforms under stress. The data are also consistent with the proposals of Deng *et al.* (*17*), which rely on stress to activate a state change from static to plastic flow conditions in glassy polymers. Deng's proposal that these events occur preferentially in localized zones containing excess free volume is entirely consistent with our observations that the relative amount of mobile nylon in the amorphous zones increases (up to the point of necking) from the very onset of deformation. Consistent with Deng's views, our data suggest that there is no real low-
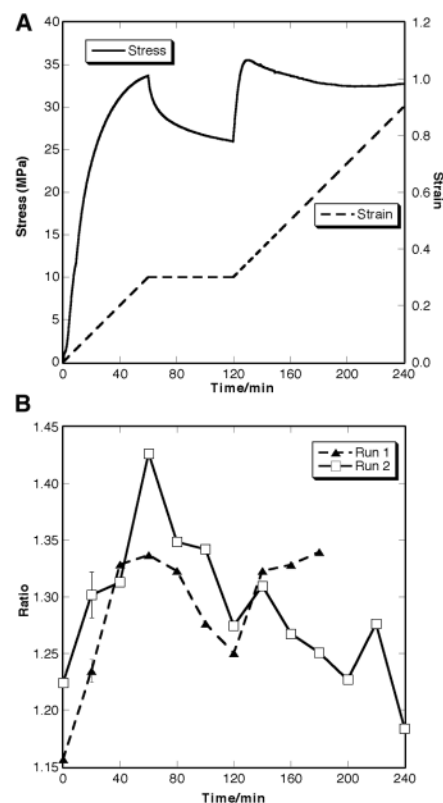
strain elastic limit for the case of tensile deformation of nylon 6 near T_g. When deformation ceased, some of the liquid-like material reverted back to the solid-like state, which results in the decreased amount of mobility. For the room-temperature experiment, the applied stress was not sufficient to bring the amorphous chains to a fictive temperature high enough to achieve the liquid-like state with motional averaging of frequency >200 kHz, which would result in a narrow ^{2}H NMR line shape. However, this result does not rule out the possibility of some mobility enhancement with a magnitude too small or dynamics too slow to be detected by deuterium NMR measurements.

References and Notes
1. A. S. Argon, in *Materials Science and Technology*, R. W. Cahn, P. Haasen, E. J. Kramer, Eds. (VCH, Weinheim, Germany, 1993), vol. 6.
2. B. Crist, in *The Physics of Glassy Polymers*, R. N. Haward and R. J. Young, Eds. (Chapman & Hall, London, 1997), pp. 155–212.
3. A. Keller and D. P. Pope, *J. Mater. Sci.* **6**, 453 (1971).
4. D. P. Pope and A. Keller, *J. Polym. Sci. Polym. Phys. Ed.* **13**, 533 (1975).
5. Z. Bartczak, A. Galeski, A. S. Argon, R. E. Cohen, *Polymer* **37**, 2113 (1996).
6. M. Utz *et al.*, *Macromolecules* **32**, 6191 (1999).
7. H. W. Spiess, *Adv. Polym. Sci.* **66**, 23 (1985).

8. D. J. Schaefer *et al.*, *Macromolecules* **28**, 1152 (1995).
9. M. T. Hansen, C. Boeffel, H. W. Spiess, *Colloid Polym. Sci.* **271**, 446 (1993).
10. L. S. Loo, R. E. Cohen, K. K. Gleason, *Macromolecules* **32**, 4359 (1999).
11. N. S. Murthy, M. Stamm, J. P. Sibilia, S. Krimm, *Macromolecules* **22**, 1261 (1989).
12. J. Hirschinger, H. Miura, A. D. English, *Macromolecules* **23**, 2153 (1990).
13. J. L. Hutchison, N. S. Murthy, E. T. Samulski, *Macromolecules* **29**, 5551 (1996).
14. E. O. Stejskal and J. Schaefer, *J. Magn. Reson.* **14**, 160 (1974).
15. D. I. Hoult and R. E. Richards, *Proc. R. Soc. London Ser. A* **344**, 311 (1975).
16. R. E. Robertson, *J. Chem. Phys.* **44**, 3950 (1966).
17. D. Deng, A. S. Argon, S. Yip, *Philos. Trans. R. Soc. London. Ser. A* **329**, 613 (1989).
18. We thank A. S. Argon for helpful discussions. This work made use of the Materials Research Science and Engineering Centers (MRSEC) Shared Facilities supported by NSF under award DMR-9400334. This work was supported primarily by the MRSEC Program of NSF under award DMR 98-08941.

Low (Sub–1-Volt) Halfwave Voltage Polymeric Electro-optic Modulators Achieved by Controlling Chromophore Shape

Yongqiang Shi,[1] Cheng Zhang,[2] Hua Zhang,[3] James H. Bechtel,[1] Larry R. Dalton,[2,4] Bruce H. Robinson,[4] William H. Steier[3]

Electro-optic (EO) modulators encode electrical signals onto fiber optic transmissions. High drive voltages limit gain and noise levels. Typical polymeric and lithium niobate modulators operate with halfwave voltages of 5 volts. Sterically modified organic chromophores have been used to reduce the attenuation of electric field poling–induced electro-optic activity caused by strong intermolecular electrostatic interactions. Such modified chromophores, incorporated into polymer hosts, were used to fabricate EO modulators with halfwave voltages of 0.8 volts (at a telecommunications wavelength of 1318 nanometers) and to achieve a halfwave voltage-interaction length product of 2.2 volt-centimeters. Optical push-pull poling and driving were also used to reduce halfwave voltage. This study, together with recent demonstrations of exceptional bandwidths (more than 110 gigahertz) and ease of integration (with very large scale integration semiconductor circuitry and ultra-low-loss passive optical circuitry) demonstrates the potential of polymeric materials for next generation telecommunications, information processing, and radio frequency distribution.

Electro-optic (EO) polymers have been under development for several years (*1*). The interest in these materials derives from the need for high-speed (wide bandwidth), low-drive-voltage, EO modulators for fiber optic communication links, in which the modulator encodes an electrical driving signal onto an optical transmission beam. Improvement in link performance depends on decreasing the halfwave voltage (V_π), because link gain is inversely proportional to V_π^2 and the noise figure is directly proportional to V_π^2 in the low-gain limit (*2*). In earlier work, Teng (*3*) demonstrated a traveling wave polymer modulator at 40 GHz. Recently, polymer modulators have been demonstrated operating at over 100 GHz and $LiNbO_3$ modulators at over 70 GHz (*3*, *4*).

However, in each case the required radio frequency (rf) drive voltage has remained persistently high ($V_\pi \sim 5$ V) (*3*, *4*). The "holy grail" of the wide bandwidth optical modulator field is a $V_\pi < 1$ volt device, which would make the distribution of millimeter wave signals via photonic techniques practical and would significantly increase the efficiency of fiber optic (and satellite) communication systems. Although the focus of this report is on improvement of V_π voltages realized for polymeric modulators, we note that implementation of clever modulator designs has permitted the extension of interaction lengths for lithium niobate modulators with a corresponding reduction in V_π (*5*). In the case of polymeric materials, current improvements reflect (and future improvements will likely continue to reflect) the development of improved materials as well as improved device concepts.

Chromophore-containing polymeric materials have held the promise of exceptionally high EO coefficients (r_{33}) through the systematic chemical design of chromophores with large hyperpolarizability (β), but unanticipated problems in translating microscopic to macroscopic

optical nonlinearity have slowed progress. Great progress has been made in understanding the molecular origins of hyperpolarizability, and many molecules exhibiting exceptional β values have been synthesized (*1*, *6*). It has, however, been difficult to incorporate these molecules into a host material with sufficient noncentrosymmetric molecular alignment to achieve device-appropriate EO activity. Recent theoretical analysis by Dalton *et al.* (*1*, *7*) has shown that the dipole-dipole interactions among chromophores makes it impossible to achieve a high degree of noncentrosymmetric order unless undesirable spatially anisotropic intermolecular electrostatic interactions are minimized by modification of the shape of chromophores to sterically inhibit such interactions. Here we report the realization of a $V_\pi \sim 0.8$ V and a $V_\pi L$ (voltage interaction length) product ~ 2.2 V·cm in optical intensity modulators using a new, structurally modified, highly nonlinear optical chromophore, CLD-1 (*8*) (Figs. 1 and 2). Recently, comparable results have been achieved by researchers at Lockheed-Martin Corporation (*9*) using an FTC-type chromophore (Figs. 1 and 2).

Traditional EO polymer modulators use a Mach-Zehnder interferometer architecture with only one arm modulated with a microstripline electrode (*3*, *10*, *11*). The V_π of such a modulator can be expressed as

$$V_\pi = \frac{\lambda h}{n^3 r_{33} L \Gamma} \qquad (1)$$

where λ is the optical wavelength, h is the gap between electrodes, n is the index of refraction, r_{33} is the EO coefficient of the polymer waveguide layer, L is the interaction length, and Γ is a modal overlap integral. Low V_π can be achieved by adjusting one or several parameters in Eq. 1. However, many factors such as reducing gap distance or increasing interaction length are limited by optical insertion loss and modulation frequency requirements. The most effective approach for low V_π is to increase the EO coefficient r_{33}, which is directly proportional (in the limit of no intermolecular electrostatic interactions) to the product of molecular dipole moment (μ) and the hyperpolarizability β with the number density N of the nonlinear chromophores in the polymer matrix. In this first-order approximation, the higher the μβ and N, the higher the EO coefficient. However, for chromophores with large dipole moments and polarizabilities (α), intermolecular electrostatic interactions among the chromophores become a

[1]TACAN Corporation, 2330 Faraday Avenue, Carlsbad, CA 92008, USA. [2]Loker Hydrocarbon Research Institute and Department of Chemistry, University of Southern California, Los Angeles, CA 90089, USA. [3]Center for Photonic Technologies, Department of Electrical Engineering, University of Southern California, Los Angeles, CA 90089, USA. [4]Department of Chemistry, University of Washington, Seattle, WA 98195, USA.